NMR and Restrained Molecular Dynamics Study of the Three-Dimensional Solution Structure of Toxin FS2, a Specific Blocker of the L-Type Calcium Channel, Isolated from Black Mamba Venom[†,‡]

Jean-Pierre Albrand,[*,§] Martin J. Blackledge,[§] Franck Pascaud,[§] Michelle Hollecker,[||] and Dominique Marion[§]

Institut de Biologie Structurale Jean-Pierre Ebel, CEA-CNRS, 38027 Grenoble Cedex 1, France, and Centre de Biophysique Moléculaire, CNRS, Rue Charles Sadron, 45071 Orleans Cedex 2, France

Received January 3, 1995; Revised Manuscript Received February 27, 1995[⊗]

ABSTRACT: The three-dimensional solution structure of toxin FS2, a 60-residue polypeptide isolated from the venom of black mamba snake (*Dendroaspis polylepis polylepis*), has been determined by nuclear magnetic resonance spectroscopy. Using 600 NOE constraints and 55 dihedral angle constraints, a set of 20 structures obtained from distance-geometry calculations was further refined by molecular dynamics calculations using a combined simulated annealing−restrained MD protocol. The resulting 20 conformers, taken to represent the solution structure, give an average rmsd of 1.2 Å for their backbone atoms, relative to the average structure. The overall resulting three-fingered structure is similar to those already observed in several postsynaptic neurotoxins, cardiotoxins, and fasciculins, which all share with toxin FS2 the same network of four disulfide bridges. The overall concavity of the molecule, considered as a flat bottomed dish, is oriented toward the C-terminal loop of the molecule. This orientation is similar to that of fasciculins and cardiotoxins but opposite to that of neurotoxins. On the basis of the local rms displacements between the 20 conformers, the structure of the first loop appears to be less well defined in FS2 than in the previously reported neurotoxin structures, but fasciculin 1 shows a similar trend with particularly high temperature factors for this part of the X-ray structure. The concave side which presents most of the positively charged residues is quite similar in FS2 and fasciculin 1. The main difference is shown by the convex side of the third loop, mostly hydrophobic in FS2, in contrast to the pair of negatively charged aspartates in fasciculin 1. This difference could be one of the factors leading to the distinct pharmacological properties—L-type calcium channel blocker for FS2 and cholinesterase inhibitor for fasciculins—observed for these two subgroups of the "*angusticeps*-type" toxins.

The venoms of snakes from the Elapidae and Hydrophidae families contain a wide variety of toxins with very distinct pharmacological properties (Ménez et al., 1992). A large proportion of these toxins falls into two classes of highly toxic small proteins composed of 60−75 residues, the neurotoxins (Endo & Tamiya, 1991) and the cytotoxins (Dufton & Hider, 1991), which have been the most extensively studied. The neurotoxins are subdivided into short (60−62 residues) and long (65−74 residues) neurotoxins. They both operate at the postsynaptic level by blocking the nicotinic receptor of acetylcholine (ACHR)[1], thus leading to flaccid paralysis of the muscle concerned (Endo & Tamiya, 1991). The cytotoxins, also known as cardiotoxins, have been found only in the cobras and ringhals families and are thought to operate at the cell membrane level, by changing the permeability and/or directly affecting the membrane organisation.

These two classes, though immunologically very distinct, have similar structures: their sequence can be easily aligned (four conserved pairs of cysteines), and they all share the same "three-fingered" architecture, as revealed by a number of X-ray and NMR structures (cf. Table 1).

Besides these two main families, a third class of postsynaptically active toxins, which are thought to have appeared later in evolution, has been isolated from the venoms of the genus *Dendroaspis* (Mamba snakes family) and grouped together under the name of *angusticeps*-type toxins (Strydom, 1976; Joubert & Taljaard, 1980a). Although structurally homologous, they show no neurotoxic or cytotoxic capability. They all have a very weak lethal character when tested alone, but a synergistic enhancement is generally observed when they are used in combination with other components of the same venom (Karlsson et al., 1985). Their homology and immunological properties have led to categorization into four subgroups (Strydom, 1977; Joubert & Taljaard, 1980a). For two of these subgroups, a well defined activity has been reported:

(1) Toxins of subgroup I are potent inhibitors of acetylcholinesterases (Karlsson et al., 1985), and the X-ray structure of one of them, fasciculin 1 from *Dendroaspis*

[†] This work (publication no. 264 of the Institut de Biologie Structurale-Jean-Pierre EBEL) was been supported by the Centre National de la Recherche Scientifique, the Commissariat à l'Energie, Atomique, and Biosym Technologies, Inc.

[‡] The coordinates of these 20 conformers have been deposited in the Brookhaven Protein Data Bank (entry code 1TFS).

* Author to whom correspondence should be addressed.

[§] Institut de Biologie Structurale-Jean-Pierre EBEL, Grenoble.

[||] Centre de Biophysique Moléculaire, Orléans, and faculty member of the Université d'Orléans.

[⊗] Abstract published in *Advance ACS Abstracts,* April 15, 1995.

[1] Abbreviations: FS2, toxin FS2; NOE, nuclear Overhauser effect; NOESY, 2D nuclear Overhauser effect spectroscopy; TOCSY, 2D total correlation spectroscopy; COSY, 2D correlation spectroscopy; P-COSY, purged COSY; PE-COSY, primitive exclusive COSY; DQF, double-quantum filtered; rmsd, root mean square deviation; rMD, restrained molecular dynamics; SA, simulated annealing; ACHR, acetylcholine nicotinic receptor.

0006-2960/95/0434-5923$09.00/0

angusticeps (green mamba), has been recently reported (Le Du et al., 1992).

(2) Subgroup III comprised initially toxin FS2 from *Dendroaspis polylepis polylepis* (Strydom, 1977) and toxin C10S2C2 from *D. angusticeps* (Joubert & Taljaard, 1980a), but recently calciseptine, another close homologue of toxin FS2, has been isolated from *D. p. polylepis* venom. Calciseptine differs from FS2 by only two residues and has been demonstrated to act as a specific blocker of the L-type calcium channel (de Weille et al., 1991). Toxin FS2 has been found to have a similar blocking effect on the calcium channels (A. Harvey, private communication), by using a protocol effective to assess the antagonist effect of the 1,4-dihydropyridine ligands on the Ca^{2+} channels (Spedding, 1982).

We have initiated the NMR study of toxin FS2 for a better understanding of the structure−activity relationship of subgroup III. Although the biological activity of calciseptine has been first reported, toxin FS2 was chosen for practical reasons: it is one of the major components of black mamba venom (Strydom, 1976), and it is known to present a synergistic effect with dendrotoxin I, a toxin from the same venom studied in our laboratories (Hollecker & Larcher, 1989; Lancelin *et al.*, 1994).

Knowing the three-dimensional structure of toxin FS2, a comparative structural study of the differences and similarities with fasciculin 1 may shed light on the different functions of the *angusticeps*-type group of toxins as well as on the phylogenetic relationship between neurotoxins, cytotoxins, and *angusticeps*-type toxins.

MATERIAL AND METHODS

Dessicated venom of *D. p. polylepis* was purchased from JABRIA B. V. (The Netherlands). Protein FS2 was purified by gel filtration on Sephadex 50, followed by two successive separations by cation-exchange chromatography on a Bio-Rex 70 column. The identity and purity of toxin FS2 was ascertained by amino acid analysis and by mass spectroscopy.

NMR samples were studied at 5−10 mM concentration in 99.96% D_2O or in 90% H_2O/10% D_2O, buffered at pH 5.3 by sodium deuteroacetate (Aldrich) at 50 mM concentration. NMR data were obtained on a Bruker AMX600 spectrometer. All two-dimensional spectra were recorded using simultaneous sampling of complex data points to achieve quadrature detection in the phase-sensitive absorption mode for both dimensions (States et al., 1982). Data recorded at different temperatures (mostly 296, 305, and 310 K) were used as needed to resolve accidental overlaps of resonances, but all the data reported here are pertinent to the 305 K data sets. NOESY spectra (Jeener et al., 1979; Macura et al., 1981) were obtained in H_2O, by combining water presaturation with a low-power selective irradiation during the relaxation delay and a jump−return sequence (Plateau & Guéron, 1982) in place of the last pulse of the NOESY sequence. In some experiments a SCUBA (Brown et al., 1988) recovery delay of 160 ms followed the low-power presaturation of water to restore the correlation with saturated H^{α}. Mixing times of 60, 100, and 150 ms were used, and a special sequence (Otting et al., 1990) was used to assess the eventual contribution of zero-quantum coherence at short mixing time. Clean TOCSY (or HOHAHA) experiments (Braunschweiler & Ernst, 1983; Davis & Bax, 1985; Griesinger et al., 1990) were performed using a WALTZ-17 (Bax, 1989) mixing sequence flanked by 2 ms purging pulses for mixing times of 80 ms. The same techniques of water suppression were used as for the NOESY experiments, the jump−return sequence being made to follow a flip back pulse (Bax, 1989). Typical two-dimensional data sets comprised 700−900 t_1 increments of 2048 data points to yield 1024 × 1024 real points matrices after zero-filling and Fourier transformation. Lorentz to Gauss transformation was used in both dimensions, and a first-order polynomial baseline correction of the transformed F_2 spectra was systematically applied before Fourier transformation in the F_1 dimension.

$^3J(H-N-C^{\alpha}-H)$ coupling constants were measured from DQF-COSY spectra (Rance et al., 1983) recorded in H_2O, with a weak water presaturation. Data sets 800 (F_1) × 4K (F_2) in size yielded a digital resolution of 0.95 Hz/point in F_2 and 3.81 Hz/point in F_1 after one time or two times zero-filling. The data were multiplied by a $\pi/4$ shifted sine-bell in F_2 and an unshifted sine-bell in the F_1 dimension.

Measurement of $^3J(H-C^{\alpha}-C^{\beta}-H)$ was carried out on PE-COSY spectra (Mueller, 1987) recorded in 99.96% D_2O . The reference 0° mixing pulse COSY time data set required to subtract from the 35° mixing pulse data set was generated from a single FID (Marion & Bax, 1988) of 8K data point recorded with 16 times more scans than the corresponding 35° COSY. First this FID was used to generate the second FID, which would be acquired with a 90° phase shift of the first pulse for F_1 quadrature detection by the States et al. (1982) method, by permuting the first and second points and negating the resulting second point for each pair of complex points in the FID. These two FIDs were then left shifted to generate the successive t_1 increments of the 0° COSY data set, which was finally subtracted with a $^1/_{16}$ scaling factor from the 35° COSY data set, yielding the PE-COSY time domain data set. This data set was then processed as described above for the DQF-COSY experiments.

Amide proton exchange rates were studied qualitatively on a sample lyophilized from H_2O and dissolved in D_2O at time zero of a succession of TOCSY and NOESY experiments (1, 2, 4, 6, 10, and 14 h) at 298 K. Amide protons were classified in three classes according to their disappearance rate (less than 1 h, more than 12 h, and intermediate).

Experimental Restraints. NOE cross peak intensities were measured on spectra recorded at 150 ms mixing time, using the tools provided in the FELIX program. They were classified in three groups, strong, medium, and weak, corresponding to upper bounds of 2.8, 3.5, and 5 Å, respectively.

The ϕ dihedral angle constraints were deduced from the $^3J(H-N-C^{\alpha}-H)$ coupling constants; for residues having $^3J(H-N-C^{\alpha}-H) > 9$ Hz, the ϕ dihedral angle was constrained between −160 and −80°, while for values smaller than 5 Hz, the allowed range was fixed between −90 and −40°.

χ_1 dihedral angles were confined to the ranges 120 to −120°, −120 to 0°, 0 to 120°, or in a few cases to a 240° range encompassing two of the three staggered conformations, depending on the stereochemical assignments of the prochiral pairs of β-protons and on the conformational preference that could be qualitatively deduced (Bartik & Redfield, 1993) for threonines, isoleucines, and valines.

For all the residues which present a slow rate of exchange of their NH proton (Figure 1), and which appeared to be engaged in a regular secondary structure through the pattern of long distance NOE (Figure 2), the corresponding NH was

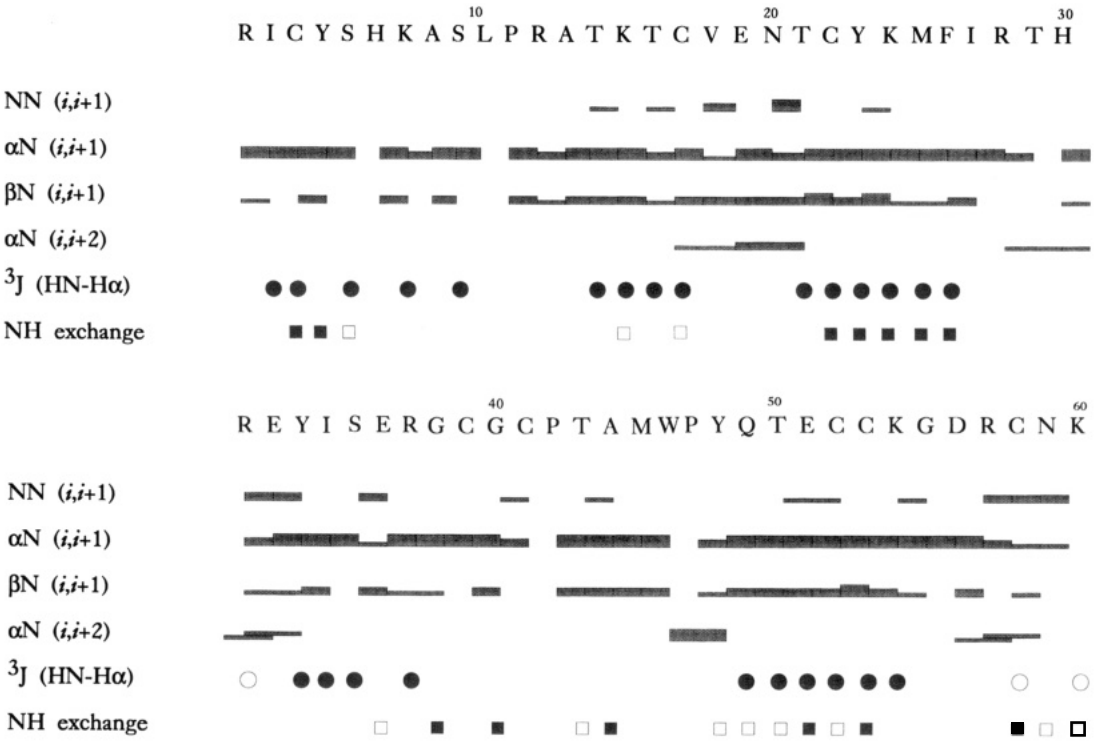

FIGURE 1: Sequential NOE connectivities, ^3J(H−N−C$^\alpha$−H) coupling constants (filled circle, ^3J(H−N−C$^\alpha$−H) > 8.5 Hz; empty circle, ^3J(H−N−C$^\alpha$−H) < 5 Hz) and chemical exchange data for the amide protons of toxin FS2 (filled square, NH detectable after 12 h exchange; empty square, NH detectable after 2 h exchange).

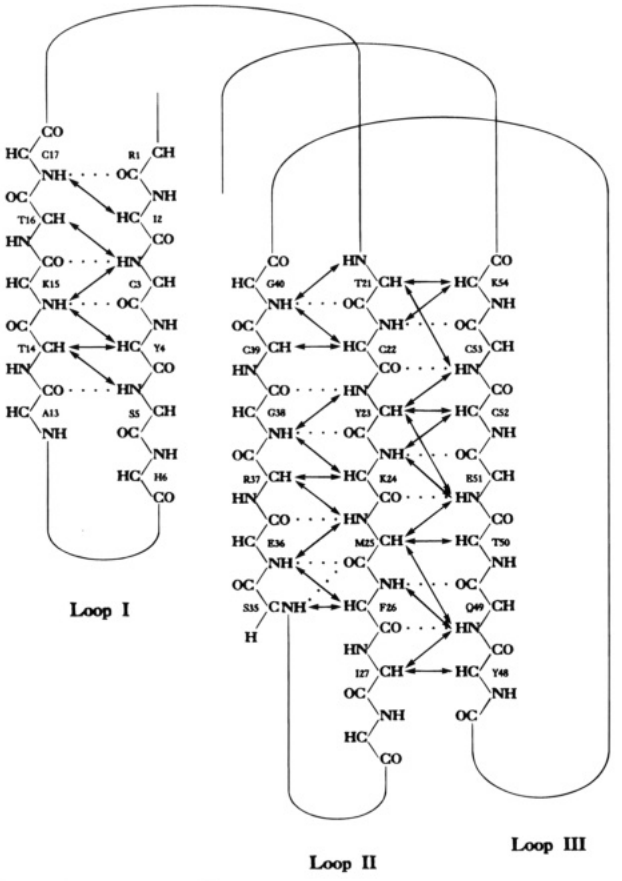

FIGURE 2: Secondary β-sheet structure of toxin FS2 deduced from the long-range NOE connectivities observed.

considered to be part of a hydrogen bond which was added as constraint with the limits 1.8−2.0 Å for the H−O′ distance and 2.8−3.0 Å for the N−O′ distance.

On the basis of the complete homology of the cysteine framework, the pairings of the disulfide bridges were assumed to be the same as those observed in neurotoxins, cytotoxins, and fasciculins (Table 1). This hypothesis was fully supported by the long range NOE data and the corresponding covalent restraints, 2.0−2.1 Å for $d(S^\gamma-S^\gamma)$ and 3.0−3.1 Å for $d(C^\beta,S^\gamma)$, were included in the restrained MD calculations.

Structure Calculations. Structure calculations were performed using the BIOSYM program DISCOVER interfaced to INSIGHTII for visualisation and analytical purposes (Biosym Technologies Inc.). The force field of AMBER4 was used in all restrained molecular dynamics calculations; in the case of the simulated annealing calculations, a quartic nonbond term was used.

Sampling of Conformational Space: Determination of Global Fold. Fifty initial structures were calculated using the distance geometry program DGII. Twenty structures were selected on the basis of the DGII error function for further calculation.

We have applied a further two-stage SA/rMD protocol (stages S_I and S_{II}, respectively) to search the local conformational space available from the experimental constraints using the 20 DGII structures as initial coordinates. This calculation does not allow complete refolding of the molecule but nevertheless allows a large sampling as previously demonstrated (Blackledge et al., 1995). The whole protocol S_I/S_{II} was applied twice for each of the initial structures; in total 40 such calculations were performed. The two-stage protocol allows a large sampling of the conformational space in the first step, followed by refinement of the structures in the presence of a more physical force field, using Lennard-Jones, Coulombic, and hydrogen-bond interactions.

Simulated Annealing Stage S_I. For the exploratory stage a simulated annealing protocol has been designed (S_I). During this period nonbonded interactions are replaced by a simple quartic repulsive term (Nilges et al., 1988; Brünger & Karplus, 1991). A switching function is initiated at 4.5

Table 1: Crystal and Solution Structures of Three-Fingered Toxins

name	species	resolution (Å)[a]	method	PDB code	reference
		Neurotoxins			
erabutoxin b	*L. semifasciata*	1.4	X-ray	3EBX	Smith et al. (1988)
erabutoxin a	*L. semifasciata*	2.0	X-ray	5EBX	Corfield et al. (1989)
erabutoxin b	*L. semifasciata*	1.7	X-ray	6EBX	Saludjian et al. (1992)
erabutoxin b	*L. semifasciata*	0.66 (14)	NMR	1FRA, 1ERA	Hatanaka et al. (1994)
α-neurotoxin	*D. p. polylepis*	0.66 (20)	NMR	1NTX	Brown et al. (1992)
toxin α	*N. nigricollis*	0.51 (8)	NMR	1NEA	Zinn-Justin et al. (1992)
cobrotoxin	*N. naja atra*	1.67 (23)	NMR		Yu et al. (1993)
neurotoxin II	*N. n. oxiana*	0.53 (19)	NMR	1NOR	Golovanov et al. (1993)
neurotoxin I	*N. n. oxiana*	1.9	X-ray		Nickitenko et al. (1993)
α-cobratoxin	*N. n. siamensis*	2.4	X-ray	1CTX	Betzel et al. (1991)
α-cobratoxin	*N. n. siamensis*		NMR		Le Goas et al. (1992)
α-bungarotoxin	*B. multicinctus*	2.5	X-ray	2ABX	Kosen et al. (1988)
α-bungarotoxin	*B. multicinctus*		NMR		Basus et al. (1988)
α-bungarotoxin complex	*B. multicinctus*		NMR		Basus et al. (1993)
κ-bungarotoxin	*B. multicinctus*	2.3	X-ray	1KBA	Dewan et al. (1994)
κ-bungarotoxin	*B. multicinctus*		NMR		Sutcliffe et al. (1992)
		Cytotoxins			
cardiotoxin V^{II4}	*N. m. mossambica*	2.5	X-ray	1CDT	Rees et al. (1990)
cardiotoxin CTX IIb	*N. m. mossambica*	0.72 (20)	NMR	2CCX	O'Connell et al. (1993)
cardiotoxin CTX V	*N. naja atra*		NMR	1CVO	Singhal et al. (1993)
cardiotoxin CTX II	*N. naja atra*	0.79 (12)	NMR	1CRF	Bhaskaran et al. (1994a)
cardiotoxin CTX III	*N. naja atra*	0.87 (20)	NMR		Bhaskaran et al. (1994b)
cardiotoxin CTX I	*N. naja atra*		NMR		Jahnke et al. (1994)
toxin γ	*N. nigricollis*	1.18 (9)	NMR		Gilquin et al. (1993)
Toxin γ	*N. nigricollis*	1.55	X-ray	1TGX	Bilwes et al. (1994)
		Fasciculins			
fasciculin I	*D. angusticeps*	1.8	X-ray	1FAS	Le Du et al. (1992)

[a] For the NMR structures, the figure given is the average backbone rmsd of all residues, with respect to the mean structure, of the (no. in parentheses) structures in the ensemble.

Å and terminated at 6.5 Å interatomic distance. Electrostatic interactions were ignored. The atomic radius was taken to be 0.825 of the van der Waals radius of the atom defined in the AMBER4 force field. For all calculations a leap-frog algorithm using steps of 1 fs was employed, and the list of neighboring atoms was updated every 20 fs. The exploratory period is calculated at a nominal temperature of 1200 K. Scaling of the various energy terms was performed as in previously published protocols (Lancelin et al., 1994; Blackledge et al., 1995). Distances were categorized as either short range or long range, so that the distances considered to determine local structure (Wüthrich, 1986) were more significant than the long range contacts in the initial stages of the calculation. In order to allow floating chirality for diastereotopic pairs, the angular term in the force field was scaled using the same factors as the nonbonded term (Weber et al., 1988).

Before the restrained MD stage the molecule is minimized for 100 steps using the steepest descent method, followed by a 3000 steps minimization using the conjugate gradients algorithm. For this step the complete AMBER4 force field described below is employed. This point in the calculation constitutes the ensemble E_I.

Restrained MD Stage S_{II}. The refinement step takes the form of a high temperature rMD calculation in which the molecule is given enough energy to overcome local energy barriers and find more favorable local conformations (S_{II}). The refinement stage of the calculation was performed using the full AMBER4 force field as implemented in the MD program DISCOVER. Nonbonded interactions contain electrostatic, van der Waals, and hydrogen bond terms. The effects of solvent were simulated implicitly using a distance-dependant dielectric (Brooks et al., 1983; Weiner et al., 1984) and reduced charges on the polar side chains (20% of their unitary force-field value, exponentially decreasing toward the end of the side chain) (Singh & Kollman, 1983). Electrostatic interactions between one and four atom pairs were scaled by a factor of 0.5. A nonbonded interaction cut-off was applied over a switching function of 1.5 Å from 8.5 to 10 Å. Electrostatic interactions are calculated using charge groups in the DISCOVER program, to avoid splitting dipoles into highly charged unphysical monopoles near the cut-off boundary.

The weight of the experimental distance constraints was reduced to 30 kcal mol^{-1} $Å^{-2}$ for the restrained MD refinement stage. The molecule was equilibrated at 600 K by assigning random atomic velocities from a Maxwellian distribution and using direct velocity scaling and temperature bath coupling during 0.5 ps. After equilibration the temperature was regulated using weak coupling to a thermal bath (Berendsen et al., 1984). The time constant for the coupling was 0.1 ps. The molecule is allowed to evolve at 600 K during 10 ps dynamic simulation, slowly cooled during 5 ps to 300 K, at which temperature the molecule evolves for a further 10 ps. Finally, the structure was minimized using conjugate gradient algorithm until the maximum derivative was less than 0.02 kcal mol^{-1} $Å^{-1}$. This ensemble will be subsequently referred to as E_{II}.

Structural Analysis. An experimental violation function V_i, representing the sum of the energetic contributions from the violated experimental constraints (calculated using k_{NOE} = 30 kcal mol^{-1} $Å^{-2}$), was used to select the 20 best structures from ensemble E_{II}. All molecules in the subensemble of "best" structures, referred to as E_{II}^{20}, satisfy the criterion V_i < 25 kcal mol^{-1}. The rms deviation of the structures was calculated over the specified atoms using the program INSIGHTII. The mean backbone structure was used for statistical characterization of the various ensembles.

Rms deviation of the backbone and side-chain dihedral angles from the ensemble means has been analyzed to quantitatively measure the backbone definition. Rms deviation of the backbone conformation from the mean was calculated using the superimposition of backbone atoms from all residues and the deviation per residue calculated from this superimposition.

Hydrogen bonding analysis was performed using the program INSIGHTII. Two atoms were considered to form a hydrogen bond if the distance was less than 2.5 Å and the hydrogen bond angle was not less than 135°.

RESULTS

Spectral Sequential Assignment. The sequential resonance assignment was conducted following well established methods (Wüthrich, 1986). COSY-DQF or P-COSY spectra, both in H_2O and D_2O, were used to discriminate direct correlations from relayed peaks also present in TOCSY spectra. Spin coupling system recognition and classification between AMX systems and longer chains were based mainly on these TOCSY spectra. AMX spin systems belonging to amino acids with an aromatic side chain could be in general identified at a later stage from the correlations observed in the NOESY spectra between their β-protons and the closest aromatic protons on the side chain. The identification of the long side-chains residues was completed through comparison of the TOCSY and COSY spectra recorded in 99.96% D_2O. For most arginine residues, this identification was confirmed by the observation of the relayed correlations with the $N^{\epsilon}H$ in the TOCSY spectra.

Several starting points for the sequential assignment were easily located by comparison with the chemical shift data published for α-neurotoxin (50% homology) of the same venom (Brown & Wüthrich, 1992). In particular the triad I2-C3-Y4, the dyad T14-K15, the tetrad G38-C39-G40-C41 have a very similar pattern of chemical shifts in these two toxins. Although most sequential $C^{\alpha}H-NH$ NOE correlations were very intense as expected for a mainly extended polypeptide chain, some difficulties were encountered for a few residues. A sequential NOE $C^{\alpha}H-NH$ was missing between Ser5 and His6, but their contiguous nature is indirectly established by their long-range NOE with Thr14 and Ala13, respectively, on the opposite side of a short antiparallel β sheet (see Figure 2). The amide proton of Arg12 was difficult to locate at 305 K due to weak TOCSY relays and due to the unexpected high field position (2.10 ppm) of the $C^{\alpha}H$ resonance. However the β- and γ-protons were more easily observed in the 315 K spectra as well as the sequential NOE peaks with the α and β protons of Pro11 and with the amide proton of Ala13. Leu10 itself showed the expected NOE correlation between its H^{α} and the H^{δ} of the *trans*-Pro11. From Ala13 to Thr29, all the sequential NOE $C^{\alpha}H-NH$ could be easily recognized, and in most cases additional correlations with the protons of the side-chain were also observed. For Tyr23, the ring proton resonances 2,6H and 3,5H are severely broadened at 305 K, due to the slow flipping of the aromatic ring. A similar broadening has been previously reported for this conserved residue in several neurotoxins (e.g., Brown & Wüthrich, 1992; Zinn-Justin et al., 1992; Golovanov et al., 1993). Between 293 and 305 K, the amide resonance of Thr29 is severely broadened and sharpens into a single line above 310 K. The complete set of TOCSY relays with the side chain were only observed at 315 K. No sequential NOE signal could be detected between the α or the side-chain protons of Thr29 and the amide proton of His30. This specific broadening of Thr29 amide proton (the α-, β-, and γ-protons do not exhibit any particular broadening compared with the neighboring residues) could be the result of some local conformational change involving directly this amide proton, but the exact nature of this process has not been elucidated. The rest of the sequential assignment is continuous from His30 to Lys60.

The original sequence of toxin FS2 (Strydom, 1977) indicated a glutamine at position 32, but our NMR data are in favor of a glutamic acid: no $N^{\epsilon}H_2$ resonances were observed, and the chemical shifts for the β and γ protons of this residue are closer to the Glu random values (Wüthrich, 1986). As for Asn20, Gln49, and Asn59, the expected correlations between the side-chains NH_2 were observed in the COSY and TOCSY spectra, and they all show NOE correlations with the β- or γ-protons of their respective side chains.

According to the patterns of sequential NOE cross peaks observed for the prolines, Pro11 and Pro42 have a *trans* peptide bond while Pro47 has the *cis* configuration. Pro47 side-chain protons display atypical chemical shifts ($C^{\alpha}H$ 3.18; $C^{\beta}H_2$ 0.22, 1.60; $C^{\gamma}H_2$ 0.67, 1.39; $C^{\delta}H_2$ 3.14, 3.21), which may be due either to the *cis* peptide linkage and/or to the shielding effect of the adjacent aromatic residues. A similar finding was reported in short chain model peptides which present the same sequence, Trp-Pro-Tyr, and which have been found to favor a type VI *cis*-proline turn (Yao et al., 1994).

The β protons of residues Cys3, Cys17, Cys22, Tyr23, Lys24, Tyr33, Arg37, Met45, Tyr48, Cys52, Cys53, and Cys58 were stereochemically assigned following criteria based on the values of the $^3J(H-C^{\alpha}-C^{\beta}-H)$ coupling constants and intraresidue NOEs (Wagner et al., 1987). A further set of residues including Tyr4, His6, Lys7, Ser9, Thr14, Lys15, Val18, Thr21, Phe26, Ile34,Cys39, Cys41, Glu51, Lys54, and Asn59 had their χ_1 dihedral angle range restrained to 120 or 240° on the basis of the qualitative method proposed by Bartik and Redfield (1993). The complete sequential assignment data for the proton resonances of toxin FS2 may be found in the Supplementary Material. Figure 1 summarizes the sequential NOE connectivities, $^3J(H-N-C^{\alpha}-H)$ and amide chemical exchange rates.

Sequential and long range NOEs ($C^{\alpha}H-C^{\alpha}H$, $NH-C^{\alpha}H$, and NH−NH) allow the identification of secondary structure elements: a short stretch of antiparallel β-sheet involving residues 1−5 and 13−17 and a triple-stranded antiparallel β-sheet involving residues 35−40, 21−27, and 48−54 (Figure 2). The two-stranded β-sheet involving residues 1−5 and 13−17 is defined like the corresponding β-sheet in homologous neurotoxins (Brown & Wüthrich, 1992; Zinn-Justin et al., 1992) by the interstrand NH−O′ hydrogen bonds 3−15, 5−13, 15−3, and 17−1, with slow or intermediate exchange rate of the corresponding amide protons. Residues Gly55, Asp56, Arg57, and Cys58 form a type II turn with a probable hydrogen bond between the slowly exchanging Cys58 NH and Gly55 O′. The other turns are not well characterized by the NOE interactions and do not fit with the classic types, although the turn involving Pro47, which has a *cis*-peptide linkage, appears in the final structures to be close to a type VIa *cis*-proline turn (Richardson, 1981).

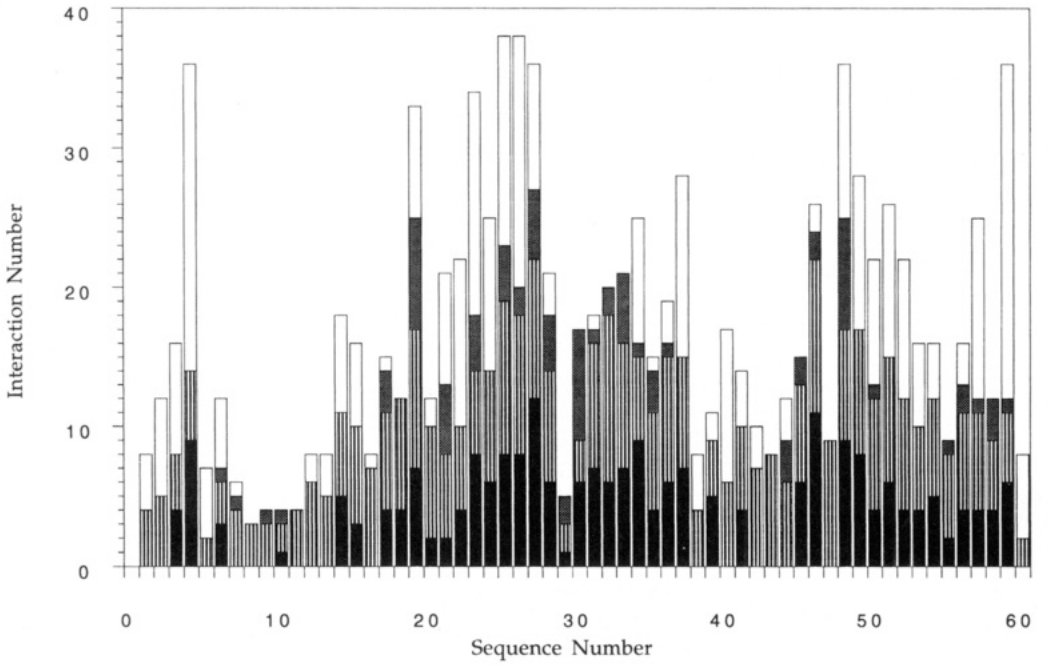

FIGURE 3: Sequential distribution and range of the NOE distance constraints used in the calculation of toxin FS2 structures. Black, intraresidue NOEs; stripes, sequential NOEs; cross-hatched, medium-range NOEs $< i + 5$; white, long-range NOEs.

As in other short toxins (cf. references in Table 1), no helical structures were observed in FS2.

Distance geometry calculations were carried out on an initial set of 350 internuclear distances, and the obtained crude structures were then used in an iterative manner to collect more constraints or reassign ambiguous ones till the final set of about 600 constraints was retained for further calculations (Figure 3). This set of distance constraints was completed by 27 ϕ and 28 χ_1 dihedral angle constraints.

Structure Determination. For the final calculations, 20 out of 50 distance geometry structures were selected on the basis of their final error in the DGII calculations. These 20 structures were used as starting structures for the two-stage simulated annealing/restrained molecular dynamics protocol S_I/S_{II}. The SA protocol has been shown to have a radius of divergence capable of sampling over 5 Å rmsd for the backbone in the initial stages of the calculation so that there is negligible dependence on the initial structure (Blackledge et al., 1995). The energetic and geometric statistics of the ensembles at the end of each stage in the calculations are shown in Table 2 and Figure 5. The rMD period S_{II} produces a systematic drop in total energy of approximately 100 kcal mol^{-1}; this energy change stems predominantly from non-bonded interactions due to reorientations of the side chains of certain residues, for example the Arg12, Ser35, and Thr29, to accommodate a more feasible structure with respect to the force field. This illustrates the fact that using high temperature rMD allows a much larger exploration of the local conformational space than is available from the simple conjugate gradients energy minimization applied to both ensembles. Despite the fact that the mean backbone conformations of the two ensembles E_I and E_{II} are very similar (rms difference = 0.23 Å), the average rmsd change for the individual conformers of the two sets, between the SA and the rMD stages of the calculation, is nevertheless 1.06 ± 0.32 Å for the backbone and 1.77 ± 0.28 Å for the heavy atoms. The divergences of the two ensembles about their mean is comparable as are the experimental error energy terms.

Table 2: Energetic and Structural Statistics of Toxin FS2

energy term	E_I	E_{II}	E_{II}^{20}
	(a) Energetic Statistics[a]		
bond	14.19 ± 4.59	13.69 ± 3.72	11.70 ± 0.78
angle	109.94 ± 31.94	106.80 ± 28.20	90.75 ± 9.35
dihedral	84.11 ± 10.34	89.06 ± 9.12	82.35 ± 5.82
out of plane	2.97 ± 1.07	3.14 ± 1.04	2.55 ± 0.50
H-bond	−27.19 ± 1.65	−31.29 ± 2.07	−30.41 ± 1.91
vdW	−159.08 ± 27.48	−177.94 ± 25.85	−185.40 ± 11.19
elec. static	−664.75 ± 16.99	−736.91 ± 25.42	−718.45 ± 14.94
total	−638.81 ± 77.27	−732.40 ± 70.16	−745.65 ± 20.77
experimental	47.13 ± 50.67	40.34 ± 32.71	20.45 ± 2.58
	(b) Structural Statistics		
BB[b] (1−60)[c]	1.24 ± 0.37	1.27 ± 0.37	1.21 ± 0.46
Heavy (1−60)	1.93 ± 0.41	1.96 ± 0.45	1.80 ± 0.43
BB (1−5, 13−60)			0.69 ± 0.15
Heavy (1−5, 13−60)			1.28 ± 0.13

[a] All values represented in kcal mol^{-1}. E_I = ensemble of 40 structures after SA stage; E_{II} = ensemble of 40 structures after rMD stage; E_{II}^{20} = 20 best structures from E_{II}. [b] Backbone atoms used for superposition (C',C^α,N). [c] Rmsd values are the average pairwise rmsd, relative to the mean of the corresponding ensemble, for the residues and atoms shown; values are given in Å.

For the 20 "best fit" structures comprising E_{II}^{20}, selected as described above, no distance violations greater than 0.41 Å and no dihedral violations greater than 5°could be observed. On average, 14.5 ± 3.4 distance violations >0.10 Å and among these 1.90 ± 1.16 > 0.2 Å are observed. Within this set no significant deviation from the idealized force field values were observed (⟨rmsd (bonds)⟩ = 0.0054 ± 0.0016 Å, ⟨rmsd (angles)⟩ = 0.75 ± 0.03°). The mean rmsd value for superimposition of the 20 conformers on their average structure is 1.2 ± 0.4 Å for the backbone atoms N,C^α, C' for all the residues, and this value falls below 0.7 ± 0.1 Å if the residues 6−12 corresponding to the poorly defined region of loop I are excluded (Table 2b and Figure 5).

Description of the Structure. As a result of the primary sequence homology, the overall fold of FS2 comes close to that of other neurotoxins and cardiotoxins as illustrated in

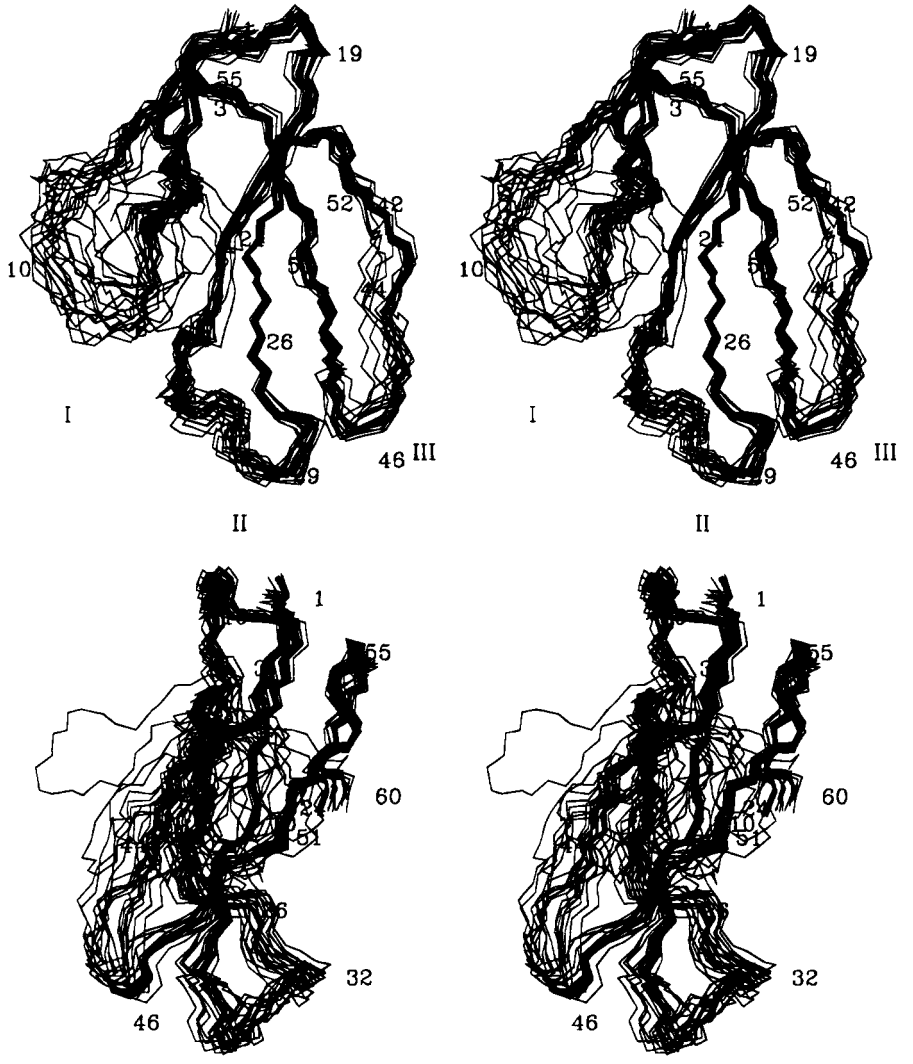

FIGURE 4: Backbone superimposition of 20 structures resulting from simulated annealing calculations of toxin FS2. The structure for which the tip of loop I sticks out in the side view is the one which has the highest energy in the set retained, but it satisfies the selection criteria based on the distance violations.

Figure 4. Three loops extending from the cross-over region are depicted: loop I (from residue 1 to 17), loop II (from residue 21 to 40), and loop III (from residue 40 to 56).

Loop I is connected to the top of loop II through an irregular extended turn (Val18 to Asn20). As a result of the lack of NOE restraints (Figure 3), its midsection (from Lys7 to Arg12) is poorly defined and cannot be precisely characterized as a regular turn: large rmsd values (>2 Å) are observed together with large dispersion of the ϕ/ψ dihedral angles (Figure 5).

Loop II is the longest and provides two of the three strands of the antiparallel β-sheet (residues 21−28 and 35−40). It is interrupted at Ser35 ($\langle\phi\rangle = -87 \pm 11°$ and $\langle\psi\rangle = -43 \pm 9°$) by a β-bulge including also Glu36 and Met25. As expected for a classic β-bulge (Richardson, 1981), Met 25 O' is involved in a bifurcated hydrogen bond with both Ser35 and Glu36 NH (Figure 9).

Loop III contributes to the third strand of the β-sheet (residues 47−53), while the downward stretch of loop III (residues 40−46) tilts the plane of loop III orthogonally to the average plane of the molecule. This loop is terminated by a type VIa *cis*-proline turn (Richardson, 1981) with a hydrogen bond between Tyr48 NH and Met45 O'.

These three loops stabilize each other by a network of hydrogen bonds. The end of loop II consists of two linked turns (from 27 to 30 and from 30 to 33). Although this part is not highly structured, a low local rmsd is observed (Figure 5): in fact, the tips of loop II and III are bound together by a hydrogen bond (Arg28 NH−O' Pro47). The two successive turns at the end of loop II appear to be represented in the calculated conformers by two distinct sets of conformations:

(1) The first (27−30) is either a type I turn (with His30 NH−O' Ile27 hydrogen bond; 10 structures) or a distorted turn with two hydrogen bonds (His30 NH−O$^{\gamma}$ Thr29 and Arg31 NH−O' Thr29; 10 other structures) (see Figure 6b,c).

(2) The second is frequently a γ turn (Richardson, 1981) with a NH(33)−O'(31) hydrogen bond and less often a conformation with a NH(33)−O'(30) hydrogen bond (four structures out of 20).

It must be emphasized that this feature of the calculations could merely result from the looseness of the NOE constraints in this region and should not be taken as a definitive evidence of multiple conformations. In particular, the hydrogen-bond network predicted by the calculations for these turns is not supported by slow exchange rates of the corresponding amide protons. It remains that the broadening of Thr29 NH, observed when the temperature is lowered, could reasonably be explained by the slowing down of the interconversion between several local conformations.

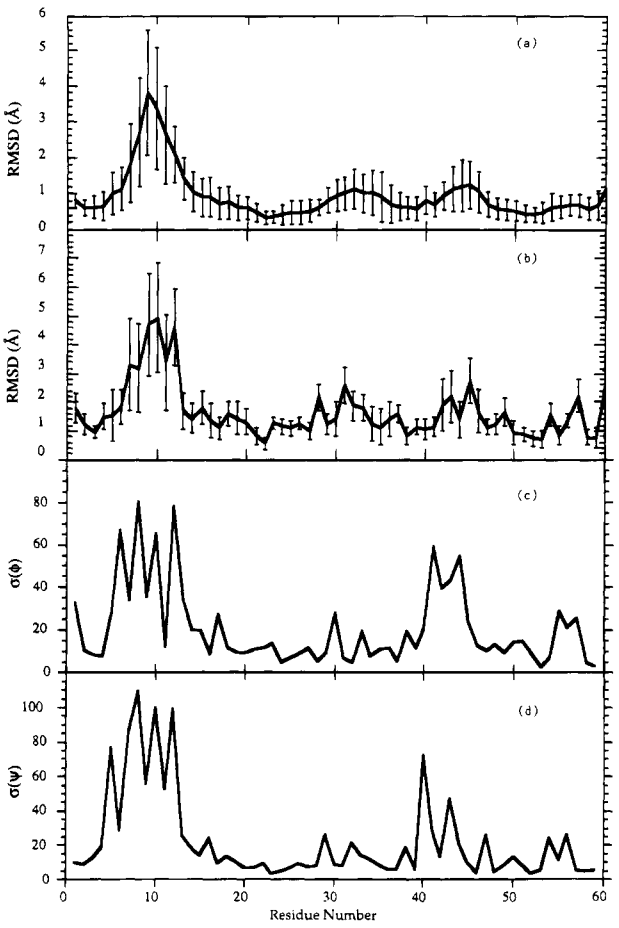

FIGURE 5: Illustration of the local deviations of the 20 calculated structures relative to the average structure: (a) Backbone atoms rmsd; (b) Side-chain heavy atoms rmsd; (c) ϕ angles standard deviation; (d) ψ angles standard deviation.

The C-terminal end of the structure is very well defined with a type II turn from residues 55 to 58 which is reinforced by the disulfide bridge 53−58 (Figure 6d). This turn is followed by a second one (57 → 60) and stabilized by the NH−O′ hydrogen bond 60−58. The head and tail of the molecule are maintained in a close proximity by the following hydrogen bonds observed in nearly all the calculated structures: Arg57 NH−O′ Ile2, Tyr4 NH−O^{δ} Asn59, Asn59 $H^{\delta 22}$−O′ Tyr4, Asn59 $H^{\delta 21}$−O′ Tyr23. Both δ-protons of Asn59 have very slow exchange rate with the solvent.

The four disulfide bridges have structural characteristics similar to those reported for α-neurotoxin of the same venom (Brown & Wüthrich, 1992), i.e., only the 53−58 bridge appears to have a nearly unique R conformation with χ_3 around +79° for 18 of the structures, while for the three other bridges there is a more or less equal distribution between the *R* and *S* conformations. Except for Cys39 and Cys41, all the cysteine β-protons were stereochemically assigned and a single χ_1 conformation is observed for all but Cys17 and Cys39.

Relation between the Hydrogen Bonds Satisfied in the Final Structures and the Observed Exchange Rates of the Amide Protons. The exchange experiments separate the amide protons into three classes: (i) Fast exchange rate, less than 2 h; (ii) medium exchange rates, 2−12 h; (iii) slow exchange, still detectable beyond 12 h (Figure 1). The slow-exchanging NHs, which fit the antiparallel β-sheet pattern, were considered part of a hydrogen bond and thus included as an explicit restraint in the molecular simulation. None of these were violated in the final structures.

The remaining three slowly exchanging NHs which are not part of the β-sheet structures are Tyr4 NH−O^{δ} Asn59, Cys58 NH−O′ Gly55, and Ala 44 NH with an unidentified partner (probably the hydroxyl of Thr43). Among the amide protons which present an intermediate exchange rate, Tyr48 is hydrogen-bonded to O′ Met45 in all the calculated structures, as expected for the type VIa *cis*-proline turn (Richardson, 1981); Asn59 NH forms an internal hydrogen bond with its O^{δ} in 11 of the structures. Three residues, Thr43, Thr50, and Cys52, have amide protons with an intermediate exchange rate although they are on the surface of the molecule on loop III and oriented toward the solvent.

In several neurotoxins and cardiotoxins, residues 50 and 52 are involved in intermolecular hydrogen bonding, which leads to dimeric association in the crystal structure (Love & Stroud, 1986; Rees et al., 1990; Betzel et al., 1991; Saludjian et al., 1992; Dewan et al., 1994) and in the case of κ-bungarotoxin, in solution (Oswald et al., 1991; Sutcliffe et al., 1992). The observation of such a dimer by NMR is made difficult by the small size of contact area (Golovanov et al., 1993) and its symmetry as well as the short life time of the dimer. A weak NOE between Cys52 NH and Cys53 H^{α} is observed for FS2 at 293 K (but no longer at 303 K) and can tentatively be interpreted as an evidence of a head-to-tail pairing at Cys-52, as for cardiotoxin $V^{II}4$ (Rees et al., 1991) or for erabutoxin-b (Saludjian et al., 1992). As the corresponding *intramolecular* distance is larger than 5 Å, a misinterpretation is not likely.

Several NH, which appear involved in intramolecular hydrogen bonds in the computed structures, are found experimentally in fast exchange: these data indicate that they remain always solvent accessible. For loop I, the least well defined part of the molecule (Figures 4 and 5), the occurrence of hydrogen bonds is statistically sparse. The hydrogen bonds reported above for the two turns of loop II (but not detected by NMR) most likely play an important role in its particular orientation: despite its flexibility, the overall local fold is conserved in the majority of the structures (Figure 6b,c). The computed hydrogen bond Arg28 NH−O′ Pro47, which links loops II and III, is not experimentally supported by the exchange rate either; this particular hydrogen bond, which is never observed in short neurotoxins (Brown & Wüthrich, 1992; Zinn-Justin et al., 1992; Golonov et al., 1993), is on the other hand generally observed in the reported structures of cytotoxins (Rees et al., 1990; O'Connell et al., 1993; Gilquin et al., 1993; Bilwes et al., 1994; Jahnke et al., 1994) and fasciculin 1 (Le Du et al., 1992).

DISCUSSION

Comparison of the Structure of FS2 with the Other Known Structures of the Three-Finger Shaped Toxins. Crystallographic or solution NMR structures (Table 1) have been established for three main classes of the three-finger shaped toxins found in the venom of the Elapidae family: (i) the neurotoxins; (ii) the cardiotoxins or cytotoxins, and (iii) one of the *angusticeps*-type toxins, fasciculin 1. The structure of FS2 is the second one reported for an *angusticeps*-type toxin, which has very different pharmacological properties compared to fasciculins. Although the different loops/fingers

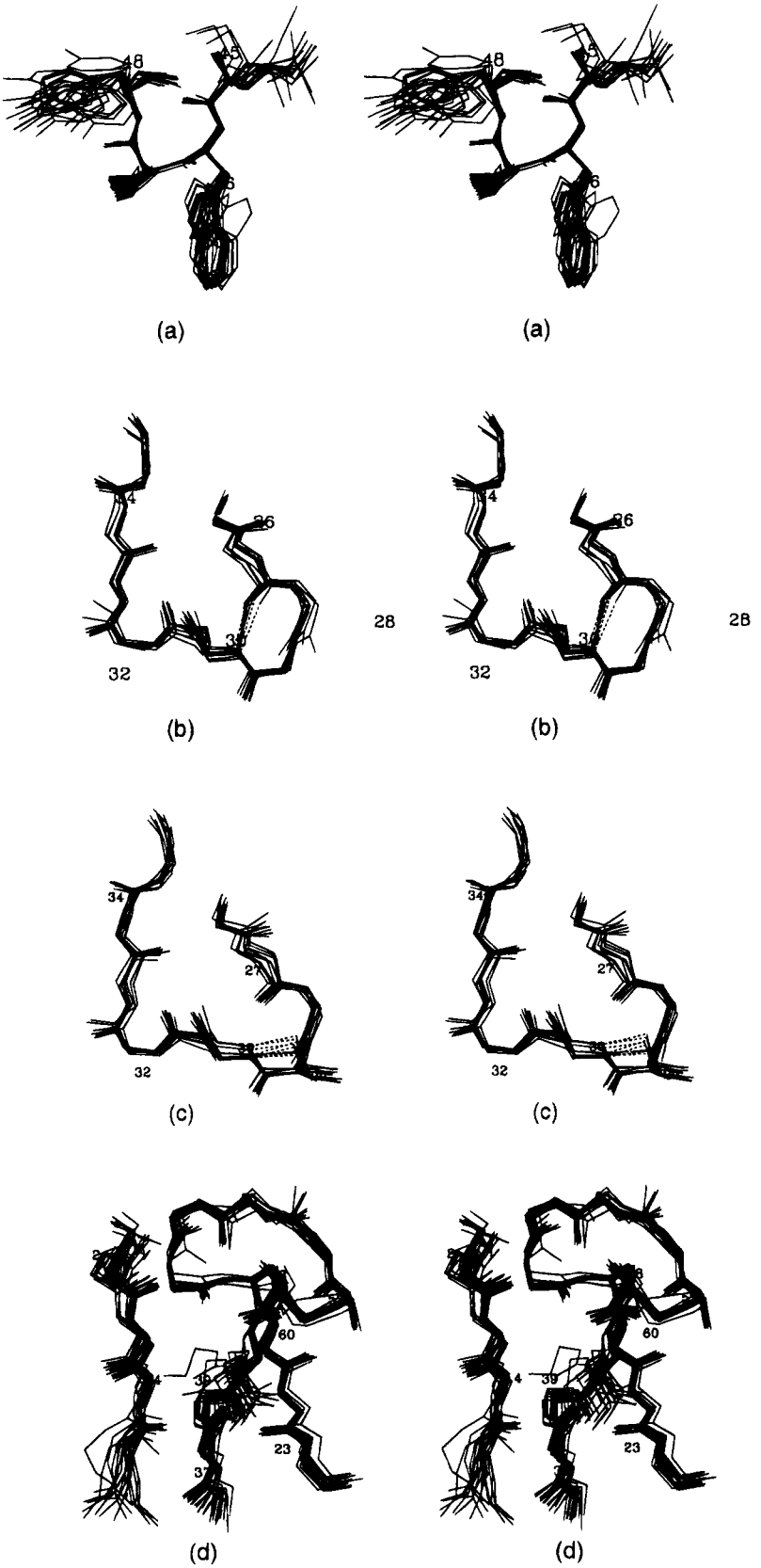

FIGURE 6: Stereoviews of selected structural elements of toxin FS2. (a) *cis*-proline turn at the tip of loop III. (b) Residues 26−35: the 10 structures with the 30 NH-O′ 27 hydrogen bond. (c) Residues 26−35: the 10 structures with the 30 NH−O$^{\gamma}$ 29 hydrogen bond. (d) Residues 1−5, 21−25, 37−39, and 53−60, in the core of the structure.

have variable lengths, their common architecture is based on a core of invariant residues (Endo & Tamiya, 1991; Dufton & Hider, 1991; Ménez et al., 1992) consisting of four pairs of cystine residues, plus Gly38 and Pro42 as well as Tyr23, Arg37, and Asn59 in nearly all sequences. For comparison with the other classes, we have used the sequence alignments of Endo and Tamiya (1991) for neurotoxins and the one used by Le Du et al. (1992) for cytotoxins. The rest of the discussion will use FS2 sequence numbering unless otherwise stated.

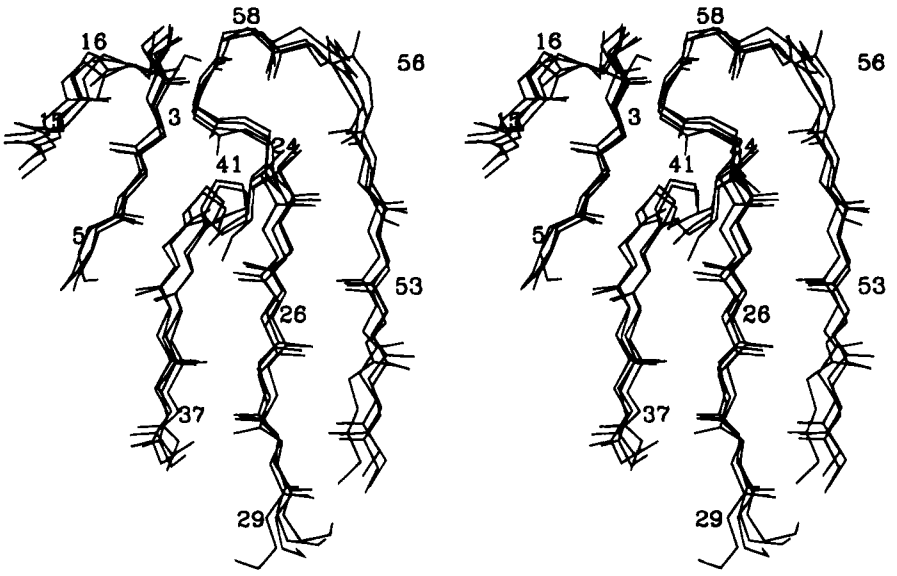

FIGURE 7: Superimposition of the conserved core region of toxin FS2, *D. p. polylepis* α-neurotoxin (1NTX), *N. m. mossambica* cardiotoxin $V^{II}4$ (1CDT), and *D. angusticeps* fasciculin 1 (1FAS). The atoms used for the superimposition are given in the text. Fasciculin 1 has an extra residue inserted after position 56.

Comparison of these different classes reveals two prominent structural features. First, the core region containing the four disulfide bridges, the top part of the β-strands, and the C-terminal loop is very similar in all these toxins, as illustrated by the backbone superimposition displayed in Figure 7. This superimposition based on residues 2−5, 14−17, 22−27, 35−39, and 49−59 of FS2 corresponds to low backbone rms differences ranging from 0.90 to 1.22 Å. Furthermore, the hydrogen bond pattern of the FS2 core is highly analogous to that of α-neurotoxin (Brown & Wüthrich, 1992). In particular, the buried side chain of the highly conserved Asn59 forms the same three interchain hydrogen bonds.

It has already been suggested that the primary function of this core is to maintain the overall structure of these three-fingered toxins (Brown & Wüthrich, 1992; Hatanaka et al., 1994). Based on this stable core, the diversity of their biological functions is achieved by the flexibility of the exposed loops, which can present a variety of arrangements of the functional residues, to fit their different targets (Ménez et al., 1992). The similarity of the core structure of toxin FS2 further supports this view and so does the recently reported structure of dendroaspin (Sutcliffe et al., 1994). The same conserved core has even been found in proteins with no related activity such as the complement regulatory protein CD59 (Kieffer et al., 1994; Fletcher et al., 1994), which belongs to a family of cell-surface molecules (Williams, 1991), whose sequences are related to the Elapid neurotoxins (Fleming et al., 1993).

Relation between the Structure of Loop II and the Overall Concavity of the Molecule. The difference in the orientation of the overall concavity of the molecule is the second important structural feature. When viewed orthogonally to the average plane, these molecules appear as an oval disk or flat dish for which a concave side can be defined facing either toward the C-terminal end—as observed in cytotoxins, fasciculins and FS2—or in the opposite direction—as observed in neurotoxins. This slight concavity is apparent in a backbone representation of the molecules (Figure 8) when viewed along the average plane. In fact, this difference of concavity results primarily from the different bend of loop II at the level of Ser35. At this location, in the postsynaptic neurotoxins, the β-sheet is extended further down toward the loop end by two or three pairs of hydrogen bonded residues, and the loop bends in the direction opposite to the C-terminal side (Figure 9). On the other hand, in the case of cytotoxins (Table 1) and of the two *angusticeps*-type toxins, including toxin FS2, there is at the same level a sharp bend of the loop end toward the C-terminal side, corresponding in most cases to a regular β-bulge (Richardson, 1981). In neurotoxins, loop II is closer to loop I than to loop III, whereas in cardiotoxins, fasciculin, and FS2, it is closer to loop III. In the former case a hydrogen bond is frequently observed with Ser8 (Figure 9) and, in the latter, between Arg28 NH and Pro47 O′.

Why do neurotoxins display a completely different fold of the central loop as opposed to other toxins? A high variability of residues 25−36 (FS2 numbering) is observed between those other toxins, but it can be noted that three highly conserved residues of neurotoxins (Trp27, Asp29, and Gly32) are always missing in the other toxins. The inherent flexibility of Gly32 may be responsible for the adoption of a particular conformation at the tip of loop II in neurotoxins.

The side-chain orientation of Arg31 (due to the different bend of loop II) may also explain why FS2 has only a very weak neurotoxic activity, maybe even no activity in absence of contaminant as for fasciculin C (Lee et al., 1985), although it is one of the most important functional groups in the binding of neurotoxins to the ACHR (Pillet et al., 1993; Fiordalisi et al., 1994). In FS2, Arg31 is relatively sheltered from the solvent on the concave side, along with all the other positively charged residues of loops II and III (Figure 11), whereas, in neurotoxins, the corresponding residue is located at the very end of loop II, in a rather exposed situation to interact with the receptor (Brown & Wüthrich, 1992; Hatanaka et al., 1994).

The local fold of the tip of loop II, which is very distinct in neurotoxins, is in contrast very similar in the three other classes of toxins, cytotoxins, fasciculins, and FS2. Thus it does not appear as a structural factor related to their specific activities. The β-bulge at position 35−36, which is observed in most structures of these three classes, does not seem

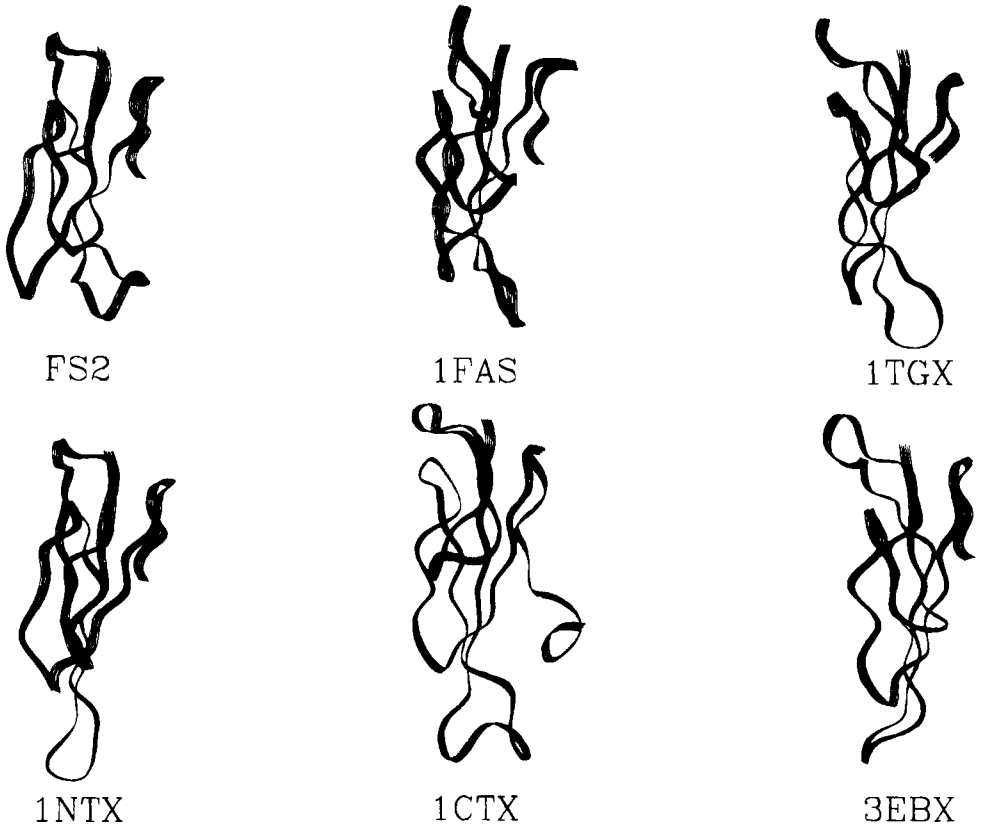

FIGURE 8: Sideways views of the ribbon structure of three neurotoxins [lower row: α-neurotoxin (1NTX, average structure), α-cobratoxin (1CTX), and erabutoxin b (3EBX)] and three nonneurotoxins [upper row: toxin FS2 (average structure), fasciculin 1 (1FAS), and *N. nigricollis* cardiotoxin γ (1TGX, conformer A)]. In the lower row the concavity of the molecules is oriented toward the left side of the picture, while in the upper row this concavity is turned toward the right side.

justified by any conserved residue in this part of the sequences; the suggestion that this bulge was due to the preceding proline in cardiotoxin γ (Gilquin et al., 1993) is not sustained by the data for FS2 and for fasciculin 1 which do not have proline at this position.

Loop III. The fold of loop III also is very similar in FS2 and in the other three-fingered toxins considered here, the main difference lying in the different type of turn at its tip. Cardiotoxins (Bilwes et al., 1994), fasciculin 1 (Le Du et al., 1992), and neurotoxins (Smith et al., 1988; Brown & Wüthrich, 1992) have nonstandard β-turns or type II turns at this location while FS2 has a type VIa *cis*-proline turn. A recent study of short model peptides (Yao et al., 1994) has shown that this type of turn is favored by the sequence Trp-Pro-Tyr, which is found in FS2 and in the other toxins from the same subgroup: calciseptine from *D. p. polylepis* (de Weille et al., 1991), toxin C10S2C2 from *D. angusticeps* (Joubert & Taljaard, 1980a), and toxin S4C8 from *Dendroaspis jamesoni kaimosae* (Joubert & Taljaard, 1980b). As observed in neurotoxins (Brown & Wüthrich, 1992; Hatanaka et al., 1994), the outer strand of loop III, which does not form any hydrogen bond with the inner strand (except for the one at the *cis*-proline turn), is not well defined by the NOE data, and the calculated structures show that several conformations can exist in this segment (Figures 4 and 5).

Loop I. As a result of the few NMR distances, the tip of loop I is poorly defined in FS2, but it should be remembered that a similar disorder is observed in the X-ray structure of fasciculin 1 (Le Du et al., 1992) or in the NMR structures of several cardiotoxins (O'Connell et al., 1993; Gilquin et al., 1993; Jahnke et al., 1994). Various situations ranging from well defined β-turns (Zinn-Justin et al., 1992; Golovanov et al., 1993; Betzel et al., 1991; Yu et al., 1993) to the lack of turns (Brown et al., 1992; Hatanaka et al., 1994) were reported for loop I in neurotoxins. If the average structure of FS2 is considered, the greatest ressemblance of loop I is with the same average region of *D. p. polylepis* α-neurotoxin (Brown & Wüthrich, 1992) (Figure 10) or erabutoxin b (Hatanaka et al., 1994). In the three toxins, His6 occupies the same buried location inside the middle of the loop, and this could explain the distension at the tip of the loop and the absence of the regular tight turn, which is observed in other neurotoxins, where this histidine is replaced by a glutamine (Zinn-Justin et al., 1992; Golovanov et al., 1993). This loop has also a similar hydrophilic character in FS2, fasciculin 1, or neurotoxins. In cytotoxins the tip of loop I is rather hydrophobic though limited by two lysine residues, and it is considered, in some cases, as a binding site to the cell membrane (Ménez et al., 1990; Dufton & Hider, 1991; Chien et al., 1994).

Differences in the Surface Charge Repartition in FS2, Cytotoxins, and Fasciculins. Whereas the neurotoxin activity can be linked to a different molecular shape, the diverse functions of the other toxins should be sought in the charge repartition and in the solvent accessibility of the three loops. All these toxins are strongly basic and positively charged at neutral pH. For cardiotoxins, however, this character is even more pronounced since, in the great majority of the known sequences (Dufton & Hider, 1991) and structures (Table 1), the few (two or three) acidic residues are confined to the structurally conserved core and the three loops all have the same composition; i.e., their tips are stretches of hydrophobic or basic residues limited by two lysines. Although a definite

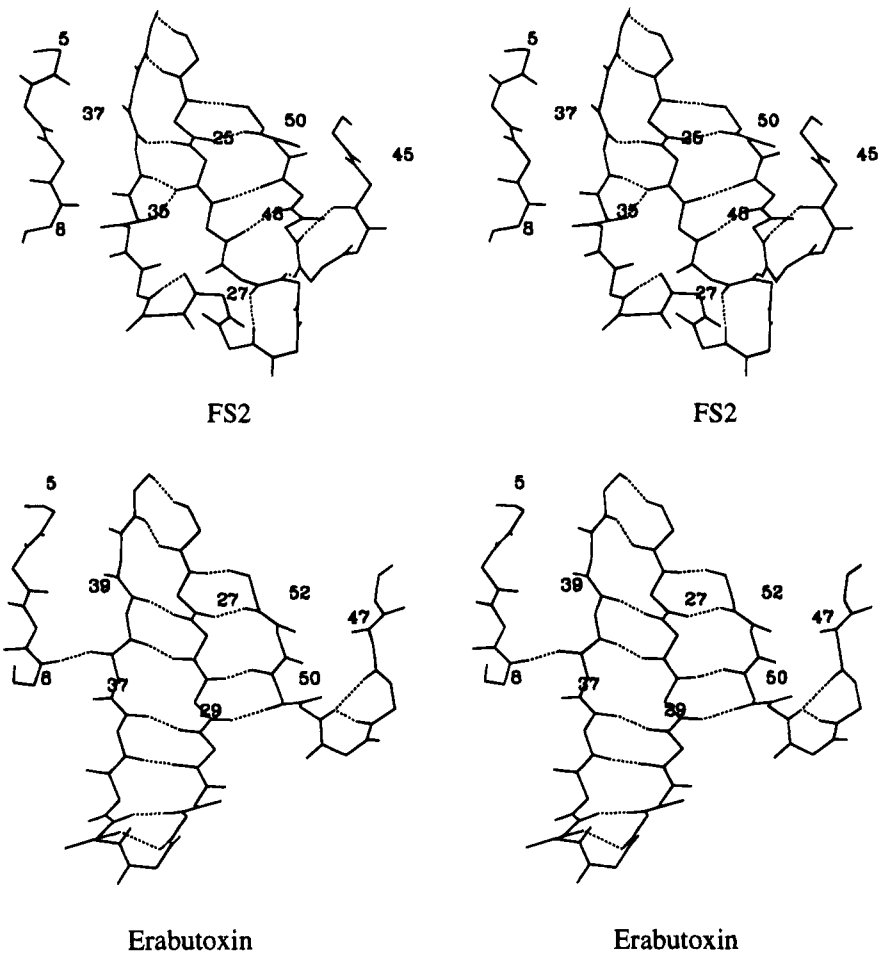

FIGURE 9: Comparison of the different bend at the tip of loop II in toxin FS2 and in the neurotoxin erabutoxin b (3EBX). In toxin FS2 the loop bends away from the viewer, starting down from residue 35 which marks the position of the β-bulge with the bifurcated hydrogen bond to O′ 25. In erabutoxin the bend down from residue 37 is toward the viewer, and the β-sheet is prolonged by three hydrogen bond (residues 25−60 of FS2 correspond to 27−62 in erabutoxin).

target has not yet been identified for the cardiotoxins (Dufton & Hider, 1991), these hydrophobic loop ends are thought to interact with the lipid chains of the phospholipid membranes and the lysine residues with their polar phosphate heads (Gilquin et al., 1993; Chien et al., 1994). In such a scheme it is not surprising that FS2 and fasciculins do not share the cytotoxicity of cardiotoxins since the corresponding segments are more hydrophilic and do not present an exclusive basic character for loop II (Glu32 and Glu36) in FS2 and for loop III (presence of Asp45 and Asp46) in fasciculins.

There are also enough differences in the charge repartition in FS2 and fasciculins to justify the lack of anticholinesterase activity observed for FS2 and its homologue C10S2C2 (Lee et al., 1985; Lin et al., 1987). While the concave sides of both molecules have a similar hydrophilic character (Arg, Asp, Lys, ..., see Figure 11), the convex sides are markedly different: a continuous hydrophobic area is observed in FS2 with Ile27, Tyr33, Met25, Tyr23, Pro42, Ala44, Met45, Trp46, Pro47, and Tyr48, while in fasciculin 1 this area is disrupted by Lys25, Arg27, Asp45, and Asp46. Furthermore, in fasciculins, loop II presents only positively charged residues (four Arg and two Lys, Figure 11), while in the case of FS2 and of the other calciseptine homologues, this positive character is reduced by several critical replacements; the neutral Met25 replaces Lys 25 and at the same time Glu36 brings a negative charge in the same location; similarly Ile27 replaces Lys27 and Glu32, Lys32. Thus in this limited area, three positive charges are replaced by two negative ones. Karlsson et al. (1985) have suggested that the dipole character of fasciculins, resulting from the contrast of the positive loop II and the negative loop III, was important for the binding to acetylcholinesterase. This view is supported by recent electrostatic calculations (Ripoll et al., 1993; Gilson et al., 1994) based on the structure of acetylcholinesterase from *Torpedo californica* (Sussman et al., 1991); they reveal the presence of a strong electrostatic dipole, aligned with the gorge leading to the active site, and they show that the access to this site is predominantly negatively charged. Under such conditions the absence of dipole character in FS2 and the presence of negative charges on its loop II should impair the binding and are probably responsible for the lack of anti-cholinesterase activity reported for toxin FS2.

Conserved Residues Which Could Explain the Common Action of Toxin FS2 and Calciseptine. Calciseptine which differs from FS2 by the two mutations Ile5Ser and Gln30His, has been demonstrated to act as a specific blocker of the L-type Ca^{2+} channel (De Weille et al., 1991). This type of voltage-activated Ca^{2+} channel is involved in the transmission of excitation signals to cardiac and smooth muscle cells and is the target of various drugs such as the 1,4-dihydropyridines, which are used in the treatment of cardiovascular disorders (Hosey & Lazdunski, 1988; Godfraind et al., 1986; Triggle & Janis, 1987). Calciseptine has been further found to share all the properties of the 1,4-dihydropyridine derivatives (Yasuda et al., 1993) and should thus have the same specific binding site at the L-type channel level. Toxin FS2

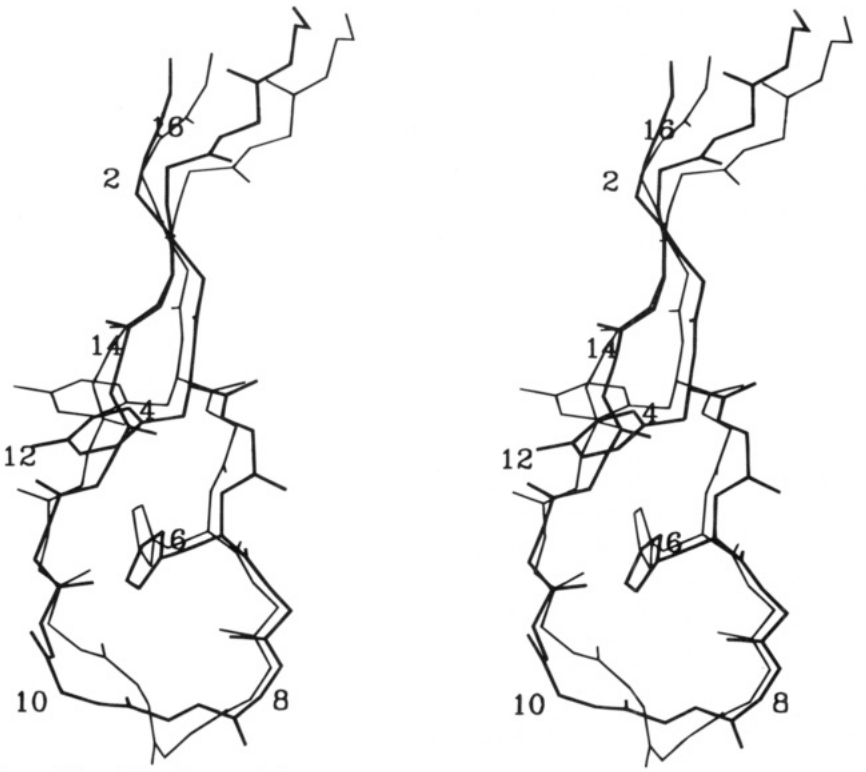

FIGURE 10: Superimposition of loop I for *D. p. polylepsis* α-neurotoxin (conformer 1) and for FS2 (conformer 10), showing the similar location of His6 and Tyr4. Note, however, that the structures chosen are the closest to the average ones, and cf. Figures 4 and 5 for the amplitude of variation at the tip of this loop.

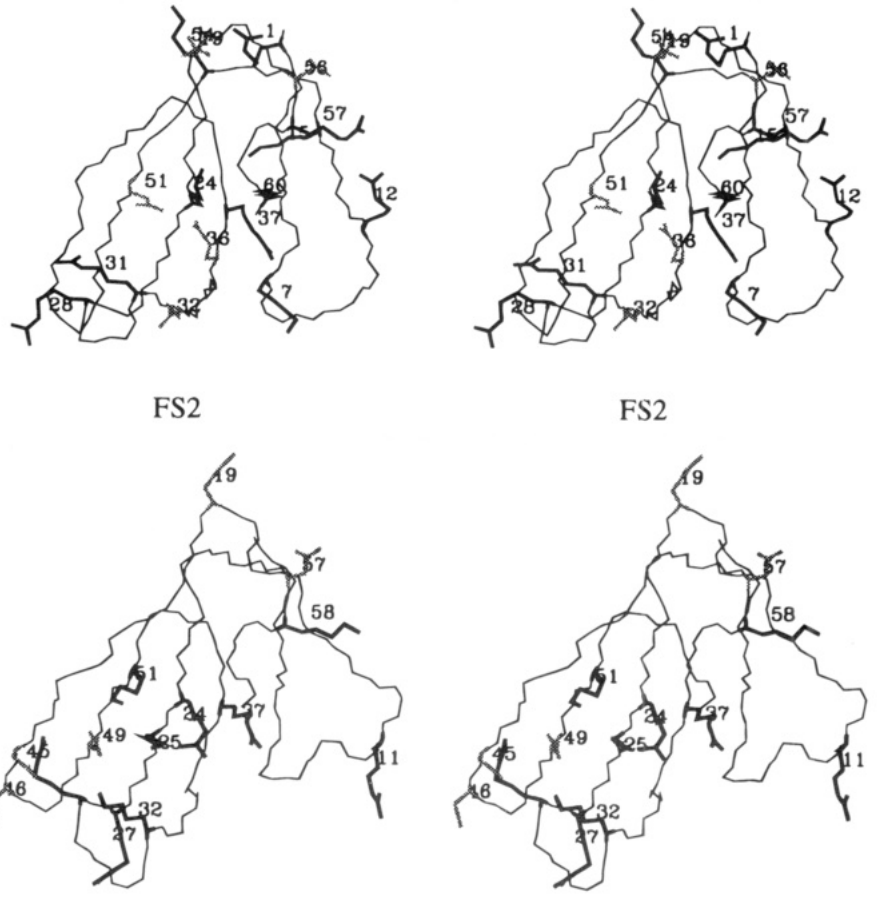

FIGURE 11: Location of the positively charged (heavy line) and negatively charged (dashed line) side-chains in toxin FS2 and fasciculin 1. The stereoviews correspond to the same orientation in both molecules with the concavity facing the viewer.

exhibits a similar blocking effect on the Ca^{2+} channel (A. Harvey, private communication), but the relative activity of calciseptine and FS2 has not been assessed precisely enough to evaluate the role of these two single-residue mutations.

However, it can reasonably be assumed that the replacement of Ile by Ser in the hydrophobic core is not important. As mentioned before, the most obviously conserved sequence which distinguish this subgroup III of the *angusticeps*-type toxins is the sequence Ala-Met-Trp-*cis*Pro-Tyr-Gln (loop III). As a result of this local conformation, the tryptophan side chain is completely exposed to the solvent (Figure 6a) and thus appears as a potential functional residue for interaction with the binding site. Two other *angusticeps*-type toxins, C10S2C2 (Joubert & Taljaard, 1980a) and S4C8 (Joubert & Taljaard, 1980b), present the same sequence and a high degree of homology with FS2 and calciseptine. Thus the key role of this conserved sequence (loop III) could be established by testing the inhibitory effect of these analogous toxins.

Evolutionary Considerations. There has been much speculation over the last two decades concerning the phylogenetic relationship of these three-fingered toxins. Early classification proposals had considered the cytotoxins as ancestors before the short and long neurotoxins (Strydom, 1973a), but this opinion has been revised (Strydom, 1973b), and it is now more often considered that cytotoxins and neurotoxins have diverged from a common ancestral form evolved from a digestive track enzyme like ribonuclease (Strydom, 1979; Dufton, 1984). On the basis of the fact that the cytotoxins occur only in the cobra and ringhals family, Dufton (1984) has suggested that they are derived from a neurotoxic ancestor after differentiation of the cobra family from the main elapid stock. Considering the structure similarity between FS2 and *D. p. polylepis* α-neurotoxin, as regard loop I and III as well as the central core, it seems obvious that they have a common ancestor and by applying the same line of argument expressed for cytotoxins, i.e., the fact that the *angusticeps*-type toxins are found only in the mamba group, it appears very probable that they have diverged from the neurotoxin branch through the loss of a few critical neurotoxic residues in the central loop. The variability of these *angusticeps*-type toxins has been attributed to their higher mutation rate (Strydom, 1977), possibly while a new useful function was sought for these toxins after the initial loss of the neurotoxic capability.

Conclusions. Toxin FS2, which is a representative of the subgroup III of the so-called *angusticeps*-type family of three-fingered toxins (Strydom, 1976), shares a common structural feature with cardiotoxins and fasciculins: the particular orientation of the concave side of the dish-shaped molecule toward the C-terminal end. This is opposite to the orientation of the same overall concavity observed in curare-mimetic neurotoxins, known to interact with the ACHR at the postsynaptic level. This difference, which results particularly from the opposite bend of the tip of loop II, probably plays an important role in the much reduced affinity of these toxins for the ACHR and the corresponding decrease in their lethal character.

Although they share a similar overall fold, particularly concerning loops II and III, these three families of toxins have little in common with regard to their mode of action, which suggests that the changes in the repartition of the charged residues on the accessible surface of the three loops play a decisive role for the recognition of their specific targets. The most remarkable structural feature, which differentiates FS2 and the other members of the subgroup III from the other *angusticeps*-type toxins, is the strong hydrophobic character of the tip of loop III. It remains to be established whether this common feature is involved in the particular affinity for the L-type calcium channel which has been observed in this subgroup.

ACKNOWLEDGMENT

We thank Pr. Alan Harvey for making his results available to us before publication and Dr. Jane Dyson for preprints of her work. We are also grateful to Drs. Eric Forest, Gilbert Hudry-Clergeon, and Jacques Ulrich, for providing us with mass spectra and HPLC data on our samples.

SUPPLEMENTARY MATERIAL AVAILABLE

One table listing the proton chemical shifts assignment and a second table listing the hydrogen bonds satisfied in the calculated structures (5 pages). Ordering information is given on any current masthead page.

REFERENCES

Bartik, K., & Redfield, C. (1993) *J. Biol. NMR 3*, 415−428.
Basus, V. J., Billeter, M., Love, R. A., Stroud, R. M., & Kuntz, I. D. (1988) *Biochemistry 27*, 2763−2771.
Basus, V. J., Song, G., & Hawrot, E. (1993) *Biochemistry 32*, 12290−12298.
Bax, A. (1989) *Methods Enzymol. 176*, 151−168.
Berendsen, H. J. C., Postma, J. P. M., van Gunsteren, W. F., DiNola, A., & Haak, J. R. (1984) *J. Chem. Phys. 81*, 3684−3690.
Betzel, C., Lange, G., Pal, G. P., Wilson, K. S., Maelicke, A., & Saenger, W. (1991) *J. Biol. Chem. 266*, 21530−21536.
Bhaskaran, R., Huang, C.-C., Tsai, Y.-C., Jayaraman, G., Chang, D.-K., & Yu, C. (1994a) *J. Biol. Chem. 269*, 23500−23508.
Bhaskaran, R., Huang, C.-C., Chang, D.-K., & Yu, C. (1994b) *J. Mol. Biol. 235*, 1291−1301.
Bilwes, A., Rees, B., Moras D., Ménez, R., & Ménez, A. (1994) *J. Mol. Biol. 239*, 122−136.
Blackledge, M. J., Medvedeva, S., Poncin, M., Guerlesquin, F., Bruschi, M., & Marion, D. (1995) *J. Mol. Biol. 245*, 661−681.
Braunschweiler, L., & Ernst, R. R. (1983) *J. Magn. Reson. 53*, 521−528.
Brooks, B. R., Broccoleri, R. E., Olafson, B. D.,States, D. J., Swaminathan, S., & Karplus, M. J. (1983) *J. Comput. Chem. 4*, 187−217.
Brown, L. R., & Wüthrich, K. (1992) *J. Mol. Biol. 227*, 1118−1135.
Brown, S. C., Weber, P. L., & Mueller, L. (1988) *J. Magn. Reson. 77*, 166−169.
Brünger, A. T., & Karplus, M. (1991) *Acc. Chem. Res. 24*, 54−61.
Cervenansky, C., Dajas, F., Harvey, A. L., & Karlsson, E. (1991) in *Snake Toxins* (Harvey, A. L., Ed.) pp 303−321, Pergamon Press, New York.
Chien, K. Y., Chiang, C. M., Hseu, Y. C., Vyas, A. A., Rule, G. S., & Wu, W. G. (1994) *J. Biol. Chem. 269*, 14473−14483.
Corfield, P. W. R., Lee, T. J., & Low, B. W. (1989) *J. Biol. Chem. 264*, 9239−9242.
Davis, D. G., & Bax, A. (1985) *J. Am. Chem. Soc. 107*, 2820−2821.
Dewan, J. C., Grant, G. A., & Sacchettini, J. C. (1994) *Biochemistry 33*, 13147−13154.
De Weille, J. R., Schweitz, H., Maes, P., Tartar, A., & Lazdunski, M. (1991) *Proc. Natl. Acad. Sci. U.S.A. 88*, 2437−2440.
Dufton, M. J. (1984) *J. Mol. Evol. 20*, 128−134.
Dufton, M. J., & Hider, R. C. (1991) in *Snake Toxins* (Harvey, A. L., Ed.) pp 259−302, Pergamon Press, New York.
Endo, T., & Tamiya, N. (1991) in *Snake Toxins* (Harvey, A. L., Ed.) pp 165−222, Pergamon Press, New York.
Fiordalisi, J. J., Al-Rabiee, R., Chiappinelli, V. A., & Grant, G. A. (1994) *Biochemistry 33*, 12962−12967.
Fleming, T. J., O'hUigin, C., & Malek, T. R. (1993) *J. Immunol. 150*, 5379−5390.

Fletcher, C. M., Harrison, R. A., Lachmann, P. J., & Neuhaus, D. (1994) *Nature Struct. Biol. 2*, 185−199.
Gilquin, B., Roumestand, C., Zinn-Justin, S., Ménez, A., & Toma, F. (1993) *Biopolymers 33*, 1659−1675.
Gilson, M. K., Straatsma, T. P., McCammon, J. A., Ripoll, D. R., Faerman, C. H., Axelsen, P. H., Silman, I., & Sussman, J. L. (1994) *Science 263*, 1276−1278.
Godfraind, T., Miller, R. J., & Wibo, M. (1986) *Pharmacol. Rev. 38*, 321−416.
Golovanov, A. P., Lomize, A. L., Arseniev, A. S., Utkin, Y., N., & Tsetlin, V. I. (1993) *Eur. J. Biochem. 213*, 1213−1223.
Griesinger, C., Otting, G., Wüthrich, K., & Ernst, R. R. (1988) *J. Am. Chem. Soc. 110*, 7870−7872.
Harvey, A. L., Anderson, A. J., Mbugua, P. M., & Karlsson, E. (1984) *J. Toxicol.-Toxin Rev. 3*, 91−137.
Hatanaka, H., Oka, M., Kohda, D., Tate, S., Suda, A., Tamiya, N., & Inagaki, F. (1994) *J. Mol. Biol. 240*, 155−166.
Hosey, M. M., & Lazdunski, M. (1988) *J. Membr. Biol. 104*, 81−105.
Jahnke, W., Mierke, D. F., Béress, L., & Kessler, H. (1994) *J. Mol. Biol. 240*, 445−458.
Jeener, J., Meier, B. H., Bachmann, P., & Ernst, R. R. (1979) *J. Chem. Phys. 71*, 4546−4553.
Joubert, F. J., & Taljaard, N. (1980a) *Biochim. Biophys. Acta 623*, 449−456.
Joubert, F. J., & Taljaard, N. (1980b) *Int. J. Biochem. 12*, 567−574.
Karlsson, E., Mbugua, P. M., & Rodriguez-Ithurralde, D. (1985) *Pharmacol. Ther. 30*, 259−276.
Kieffer, B., Driscoll, P. C., Campbell, I. D., Willis, A. C., van der Merwe, P. A., & Davis, S. J. (1994) *Biochemistry 33*, 4471−4482.
Lancelin, J.-M., Foray, M.-F., Poncin, M., Hollecker, M., & Marion, D. (1994) *Nature Struct. Biol. 1*, 246−250.
Le Du, M. H., Marchot, P., Bougis, P. E., & Fontecilla-Camps, J. C. (1992) *J. Biol. Chem. 267*, 22122−22130.
Lee, C. Y., Tsai, M. C., Tsaur, M. L., Lin W. W., Carlsson, F. H. H., & Joubert, F. J. (1985) *J. Pharmacol. Exp. Ther. 233*, 491−498.
Lin, W. W., Lee, C. Y., Carlsson, F. H. H., & Joubert, F. J. (1987) *Asia Pacific J. Pharmacol. 2*, 79−85.
Le Goas, R., LaPlante, S. R., Mikou, A., Delsuc, M.-A., Guittet, E., Robin, M., Charpentier, I., & Lallemand, J.-Y. (1992) *Biochemistry 31*, 4867−4875.
Love, R. A., & Stroud, R. M. (1986) *Protein Eng. 1*, 37−46.
Low, B. W., Preston, H. S., Sato, A., Rosen, L. S., Searl, J. E., Rudko, A. D., & Richardson, J. S. (1976) *Proc. Natl. Acad. Sci. U.S.A. 73*, 2991−2994.
Macura, S., Hyang, Y., Suter, D., & Ernst, R. R. (1981) *J. Magn. Reson. 43*, 259−281.
Marion, D., & Bax, A. (1988) *J. Magn. Reson. 80*, 528−533.
McDowell, R. S., Dennis, M. S., Louie, A., Shuster, M., Mulkerrin, M. G., & Lazarus, R. A. (1992) *Biochemistry 31*, 4766−4772.
Ménez, A., Gatineau, E., Roumestand, C., Harvey, A. L., Mouawad, L., Gilquin, B., & Toma, F. (1990) *Biochimie 72*, 575−588.
Ménez, A., Bontems, F., Roumestand, C., Gilquin, B., & Toma, F. (1992) *Proc. R. Soc. Edinburgh 99B(1/2)*, 83−103.
Mueller, L. (1987) *J. Magn. Reson. 72*, 191−196.
Nickitenko, A. V., Michailov, A. M., Betzel, Ch., & Wilson, K. S. (1993) *FEBS Lett. 320*, 111−117.
Nilges, M., Clore, G. M., & Gronenborn, A. M. (1988). *FEBS Lett. 239*, 129−136.
O'Connell, J. F., Bougis, P. E., & Wüthrich, K. (1993) *Eur. J. Biochem. 213*, 891−900.
Oswald, R. E., Sutcliffe, M. J., Bamberger, M., Loring, R. H., Braswell, E., & Dobson, C. M. (1991) *Biochemistry 30*, 4901−4909.
Otting, G., Orbons, L. P. M., & Wüthrich, K. (1990) *J. Magn. Reson. 89*, 423−430.
Pillet, L., Trémeau, O., Ducancel, F., Drevet, P., Zinn-Justin, S., Pinkasfeld, S., Boulain, J.-C., & Ménez, A. (1993) *J. Biol. Chem. 268*, 909−916.
Plateau, P., & Guéron, M. (1982) *J. Am. Chem. Soc. 104*, 7310−7311.
Rance, M., Sørensen, O. W., Bodenhausen, G., Wagner, G., Ernst, R. R., & Wüthrich, K. (1983) *Biochem. Biophys. Res. Commun. 117*, 479−485.
Rees, B., Bilwes, A., Samama, J. P., & Moras, D. (1990) *J. Mol. Biol. 214, 281*−297.
Richardson, J. (1981) *Adv. Protein Chem. 34*, 167−330.
Ripoll, D. R., Faerman, C. H., Axelsen, P. H., Silman, I., & Sussman, J. L. (1993) *Proc. Natl. Acad. Sci. U.S.A. 90*, 5128−5132.
Saludjian, P., Prangé, T., Navaza, J., Ménez, R., Guilloteau, J. P., Riès-Kautt, M., & Ducruix, A. (1992) *Acta Crystallogr. B48*, 520−531.
Singh, U. C., & Kollman, P. A. (1983) *J. Comput. Chem. 5*, 129−145.
Singhal, A. K., Chien, K.-Y., Wu, W.-g., & Rule, G. S. (1993) *Biochemistry 32*, 8036−8044.
Smith, J. L., Corfield, P. W. R., Hendrickson, W. A., & Low, B. W. (1988) *Acta Crystallogr. Sect. A 44*, 357−368.
States, D. J., Haberkorn, R. A., & Ruben, D. J. (1982) *J. Magn. Reson. 48*, 286−292.
Strydom, D. J. (1973a) *Comp. Biochem. Physiol. B44*, 269−281.
Strydom, D. J. (1973b) *Syst. Zool. 22*, 596−608.
Strydom, D. J. (1976) *Eur. J. Biochem. 69*, 169−176.
Strydom, D. J. (1977) *Eur. J. Biochem. 76*, 99−106.
Strydom, D. J. (1979) in *Snake Venoms, Handbook of Experimental Pharmacology* (Lee, C. Y., Ed.) Vol. 52, pp 258−275, Springer-Verlag, Berlin.
Sussman, J. L., Harel, M., Frolow, F., Oefner, C., Goldman, A., Toker, L., & Silman, I. (1991) *Science 253*, 872−879.
Sutcliffe, M. J., Dobson, C. M., & Oswald, R. E. (1992) *Biochemistry 31*, 2962−2970.
Sutcliffe, M. J., Jaseja, M., Hyde, E. I., Lu, X., & Williams, J. A. (1994) *Nature Struct. Biol. 1*, 802−807.
Triggle, D. J., & Janis, R. A. (1987) *Annu. Rev. Pharmacol. Toxicol. 27*, 347−369.
Tsernoglou, D., & Petsko, G. A. (1976) *FEBS Lett. 68*, 1−4.
Tsernoglou, D., & Petsko, G. A. (1977) *Proc. Natl. Acad. Sci. U.S.A. 74*, 971−974.
Wagner, G., Braun, W., Havel, T. F., Schaumann, T., Go, N., & Wüthrich, K. (1987) *J. Mol. Biol. 196*, 611−639.
Weber, P. L., Morrison, R., & Hare, D. (1988) *J. Mol. Biol. 204*, 483−487.
Weiner, S. J., Kollman, P. A., Case, D. A., Singh, U. C., Ghio, C, Alagona, G., Profeta, S., & Weiner, P. (1984) *J. Am. Chem. Soc. 106*, 765−784.
Williams, A. F. (1991) *Cell Biol. Int. Rep. 15*, 769−777.
Wüthrich, K. (1986) *NMR of Proteins and Nucleic Acids*, John Wiley, New York.
Yao, J., Feher, V. A., Espejo, B. F., Reymond, M. T., Wright, P. E., & Dyson, H. J. (1994) *J. Mol. Biol. 243*, 736−753.
Yasuda, O., Morimoto, S., Chen, Y., Jiang, B., Kimura, T., Sakakibara, S., Koh, E., Fukuo, K., Kitano, S., & Ogihara, T. (1993) *Biochem. Biophys. Res. Commun. 194*, 587−594.
Yu, C., Bhaskaran, R., Chuang, L.-C., & Yang, C.-C. (1993) *Biochemistry 32*, 2131−2136.
Zinn-Justin, S., Roumestand, C., Gilquin, B., Bontems, F., Ménez, A., & Toma, F. (1992) *Biochemistry 31*, 11335−11347.

BI950008Z